Journal of Civil Engineering and Construction 2019;8(2):55-62
https://doi.org/10.32732/jcec.2019.8.2.55

Interaction Diagram of Rubberised Concrete Filled Square Hollow Sections

Mohamed Elchalakani, Minhao Dong, Ali Karrech

School of Civil, Environmental and Mining Engineering, The University of Western Australia, Perth WA 6009, Australia
E-mail: mohamed.elchalakani@uwa.edu.au, minhao.dong@uwa.edu.au, ali.karrech@uwa.edu.au

Received: 5 September 2018; Accepted: 26 September 2018; Available online: 1 March 2019

Abstract: Rubberised concrete utilises waste material, prevents resource extraction and improves concrete ductility, however at the cost of reduced strength and stiffness. The performance of thirty rubberised concrete-filled single-skin steel tubes under combined loading conditions were systematically investigated and comparisons against six steel hollow tubular columns and beams were made. The experimental program consisted of three rubber replacement ratios, 0%, 15% and 30%, three load eccentricities and four tube sections with section slenderness (*b/t*, width/thickness) of 18 to 50. The results showed that the confined rubberised concrete and the restrained steel tube improved strength and ductility of the composite section. The rubberised concrete was more effective in delaying the premature buckling failure of the steel tube compared to the more brittle normal concrete. The rubberised concrete with 15% rubber replacement ratio showed a good balance of strength and ductility. The interaction diagrams obtained from the experiments and theoretical calculations were constructed and compared. The behaviours of the rubberised concrete filled steel tubes could be accurately predicted using existing design guidelines and safe designs can be produced. This study demonstrated the possibility of using rubberised concrete as a cost-effective solution to problems that require high moment and deformation capacity, such as the roadside barriers and columns in buildings located in seismic active zones.
Keywords: Rubberised concrete; Concrete-filled single-skin tubes; Combined loading; Interaction diagram**.**

1. Introduction

Waste tyre is an environmental, health and fire hazard, which costs millions of dollars to dispose every year [1,2]. Studies [3–5] were carried out to explore the option of using waste tyre chips or crumbs as aggregates in concrete. It was shown that the rubberised concrete (RuC) has improved mechanical properties such as ductility, fracture toughness and energy absorption compared to the normal concrete (NC), however at the cost of reduced compressive strength and stiffness. To mitigate the significant reduction in strength, RuC could be confined by steel hollow tubular sections. It is widely accepted that the concrete filled steel tubes (CFST) have significantly improved compressive and flexural strength, as well as higher ductility and energy absorption capabilities [3,4,6]. Morino et al. [7] concluded that the local buckling of the steel tubes was delayed by the concrete infill and the lateral confinement increased the strength of the encased concrete.

Currently, the rigid concrete roadside barrier does not deform sufficiently upon impact and causes injuries or fatalities to the motorists, whereas the flexible roadside barriers made of steel hollow tubes do not provide sufficient support to the vehicles due to its tendency to buckle prematurely. The rubberised CFST (RuCFST) could be potentially used as a new type of roadside barriers, or as structural members in seismic active regions. However, to the authors' best knowledge, no studies have investigated the behaviour of rubberised CFST (RuCFST) members under combined loading.

2. Experimental program

General purpose ordinary Portland cement was used as the binder material. Three mixes were compared in this study, namely NC (normal concrete), RuC15, RuC30 to denote the replacement ratios of rubber particles to aggregates. The particle size distribution curves of sand, coarse aggregates and rubber particles are shown in Fig. 1. It can be seen that 2-5 mm crumb rubber was suitable to partially replace <4 mm aggregates whereas 5-7 mm chip rubber was suitable to replace 7 mm coarse aggregates. The crumb and chip rubber used in this study were treated with 10% sodium hydroxide (NaOH) solution for 24 hours to increase bonding with cement matrix and increase its specific weight [8]. The mix proportions are shown in Table 1. A water to cement ratio of 0.48 was adopted to ensure satisfactory workability.

Table 1. Mix proportions of NC, RuC15 and RuC30

Mix	Water (kg/m^3)	Cement (kg/m^3)	Fine aggregate (kg/m^3)	10 mm coarse aggregate (kg/m^3)	7 mm coarse aggregate (kg/m^3)	<4mm Coarse aggregate (kg/m^3)	7-10 mm rubber chip (kg/m^3)	2-5 mm rubber crumb (kg/m^3)	Concrete compressive strength f'_c (MPa)
NC	205	426	843	444	306	130	0	0	40.8
RuC15	205	426	648	311	214	91	45	58	17.9
RuC30	205	426	453	178	122	52	90	117	9.5

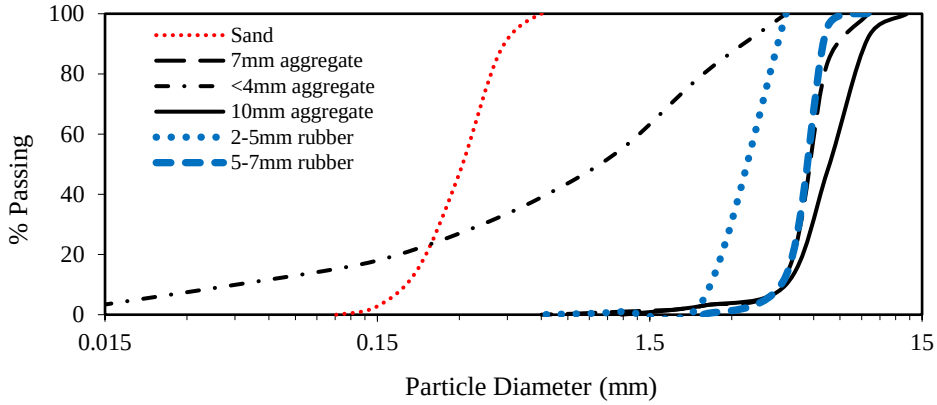

Fig. 1 Particle size distribution of the fine, coarse and rubber aggregates

Four grade C350L0 cold-formed steel sections were used for CFST beams and columns. In total, the behaviours of 18 CFST columns (2 sections, 3 types of concrete and 3 load eccentricities) and 12 CFST beams (4 sections and 3 types of concrete) were investigated. The specimen designation followed steel tube depth-steel tube thickness-load eccentricity (or "F" for the flexural tests)-rubber replacement ratio. "CFT" was used to represent concrete filled tube composite sections and "SHS" represented hollow square hollow section (SHS) members. The section slenderness, as per AS 4100 [9], of a steel tube depends on d/t, where d is the depth of the steel tube and t is the thickness. The sections were selected to be representative to the three typical types of slenderness (λs), namely compact ($\lambda s \leq 30$), non-compact ($30 < \lambda s \leq 40$) and slender ($\lambda s > 40$). The details of the SHS tubes, including slenderness classifications from AS 4100 [9] and comparison to the provisions in Eurocode 3 [10] are shown in Table 2. The composite specimens were covered with plastic sheet to limit drying shrinkage and cured for one month at ambient room temperature inside the Structural Laboratory at University of Western Australia.

Table 2. Details of the SHS tubes

Section	Depth d (mm)	Thickness t (mm)	External radius r_{ext} (mm)	Internal radius r_{int} (mm)	Area of steel A_s (mm^2)	Area of concrete A_c (mm^2)
SHS89×5	89	5	12.5	7.5	1594	6193
SHS89×3.5	89	3.5	8.75	5.25	1155	6700
SHS100×3	100	3	6	3	1141	8828
SHS100×2	100	2	4	2	774	9213
Section	Section Slenderness b/t	Section Slenderness $\frac{b-2t}{t}\sqrt{\frac{f_y}{250}}$ AS 4100 [9]	Section Slenderness $\frac{b-2r_{ext}}{t}\sqrt{\frac{f_y}{235}}$ Eurocode 3 [10]	Section Slenderness AS4100 [9]	Section Slenderness Eurocode 3 [10]	
SHS89×5	18	18.7	15.6	Compact	Class 1	
SHS89×3.5	25	27.7	24.9	Compact	Class 1	
SHS100×3	33	37.1	35.8	Non-compact	Class 2	
SHS100×2	50	56.8	56.1	Slender	Class 3	

The CFST columns were subjected to concentric and eccentric loading by a 600 kN Baldwin testing machine. The load eccentricity was the distance between the centre of the base place and the centre of the column. Four-point bending tests were adopted to measure the flexure strength of the SHS tubes and CFST beams. Each specimen was setup on the Baldwin compression machine with 100 mm overhanging segments from each end of the beam and 267 mm distance between each loading/support points.

3. Results and discussion

3.1. Strength and ductility

The 28-day compressive strengths for NC, RuC15 and RuC30 were 40.8, 17.9 and 9.5 MPa, respectively. The replacement of aggregates by rubber resulted in significant strength loss, with 15% rubber replacement reducing the strength by 56% and 30% replacement by 77%.

The strength and ductility results of the 36 concrete filled and hollow tubular specimens are shown in Table 3. The concrete contribution was calculated with respect to the load capacities of the corresponding hollow tube results and reported in this table. Overall, the concrete infill significantly improved the load carrying capacity of the hollow tubes by delaying the buckling failure. By comparing the CFST columns, it can be seen that, a lower load eccentricity, a lower rubber replacement ratio and a more compact cross-section would correspond to a greater load carrying capacity. They are due to the lower moment compared to axial load, higher concrete compressive strength, and better lateral confinement and resistance to buckling. With the confinement of steel tubes, the difference in strength among the three types of concrete was reduced. On average, the RuC15 and RuC30 filled steel tubes were 22% and 29% weaker, respectively, than those filled with the higher strength NC. This showed RuCFST had adequate strength to be used as structural members.

Ductility of the specimens was by Ductility Index (DI), which is measured between the axial displacements at 10% reduction of the failure load before and after the peak (eq. 1). The ductility results were also reported in Table 3. RuCFST also showed superior ductility performances over their NC counterparts.

$$DI = \frac{\delta_2 - \delta_1}{\delta_1} \tag{1}$$

3.2. Interaction diagrams

The interaction diagrams of concrete filled SHS89×3.5 and SHS100×3 specimens were constructed in accordance to Eurocode 4 [11] and CIDECT [12]. The four points (A-D) on the interaction diagrams were illustrated in Fig. 2. At pure compression (Point A), $M_A = 0$ and N_A is from eq. 2.

$$N_A = N_{pl,Rd} = A_c f_c' + A_s f_y \tag{2}$$

At pure bending (Point B) from Eurocode 4 [11], $N_B = 0$ and M_B was obtained from eq. 3. α_c was taken as 1 to account for the confinement by the steel tube.

$$M_B = M_{pl,Rd} = \left(W_{pa} - W_{pa,n}\right) f_y + 0.5\left(W_{pc} - W_{pc,n}\right)\alpha_c f_c \tag{3}$$

Where

$W_{pc} = \frac{(b-2t)(h-2t)^2}{4} - \frac{2}{3}r_{int}^3 - r_{int}^2(4-\pi)\left(\frac{h}{2} - t - r_{int}\right)$;

$W_{pa} = \frac{bh^2}{4} - \frac{2}{3}(r_{int}+t)^3 - (r_{int}+t)^2(4-\pi)\left(\frac{h}{2} - t - r_{int}\right) - W_{pc}$;

$W_{pc,n} = (b-2t)h_n^2$;

$W_{pa,n} = bh_n^2 - W_{pc,n}$; and

$h_n = \frac{A_c f_c'}{2bf_c' + 4t(2f_y - f_c')}$.

The Point B from CIDECT [12] was defined as eq. 4, which required to obtain a coefficient $m_{\square}$ for SHS.

$$M_{pl,Rd} = m_{\square}\frac{h^2 b - (h-2t)^2(b-2t)}{4} f_y \tag{4}$$

Point C and Point D formed an equilateral triangle on the interaction diagram. The moment at Point C was the same as that at Point B, however its load was defined as eq. 5.

$$N_c = N_{pm,Rd} = A_c \alpha_c f_c' \tag{5}$$

Table 3. Test results of the 36 concrete filled and hollow tubular columns and beams

Specimen Type	Specimen Designation	Eccentricity (mm)	Rubber replacement ratio (%)	Peak load (kN)	Ductility Index (*DI*)	Displacement at peak load (mm)	Maximum displacement (mm)	Concrete contribution ΔP_c (kN)	Concrete contribution $\%\Delta P_c$
	SHS89×3.5-0	0	-	526	1.06	10.7	41.8	-	-
	CFT89×3.5-0-0	0	0	816	1.19	7.0	45.0	+290	+55%
	CFT89×3.5-0-15	0	15	667	1.65	7.8	71.6	+141	+27%
	CFT89×3.5-0-30	0	30	588	1.77	10.2	60.8	+62	+12%
SHS89×3.5 columns	CFT89×3.5-22.5-0	22.5	0	420	1.36	5.3	59.9	-	-
	CFT89×3.5-22.5-15	22.5	15	344	1.83	5.3	74.0	-	-
	CFT89×3.5-22.5-30	22.5	30	326	2.36	4.9	97.4	-	-
	CFT89×3.5-45-0	45	0	302	1.65	7.3	61.1	-	-
	CFT89×3.5-45-15	45	15	242	2.38	6.5	113.6	-	-
	CFT89×3.5-45-30	45	30	229	2.64	7.2	72.7	-	-
	SHS100×3-0	0	-	428	0.30	5.1	55.2	-	-
	CFT100×3-0-0	0	0	854	0.98	6.4	70.4	+426	+100%
	CFT100×3-0-15	0	15	641	1.53	6.3	97.1	+213	+50%
	CFT100×3-0-30	0	30	549	1.59	6.3	49.3	+121	+28%
SHS100×3 columns	CFT100×3-25-0	25	0	492	0.95	4.9	52.1	-	-
	CFT100×3-25-15	25	15	345	1.56	5.6	55.3	-	-
	CFT100×3-25-30	25	30	309	1.57	5.4	52.8	-	-
	CFT100×3-50-0	50	0	319	1.51	6.9	51.2	-	-
	CFT100×3-50-15	50	15	259	1.94	6.7	77.7	-	-
	CFT100×3-50-30	50	30	235	1.61	7.5	85.7	-	-
	SHS89×5-F	F	-	173	2.32	20.1	54.8	-	-
SHS89×5 beams	CFT89×5-F-0	F	0	207	12.03	38.9	145.4	+34	+19%
	CFT89×5-F-15	F	15	199	10.49	39.6	117.4	+26	+15%
	CFT89×5-F-30	F	30	194	7.90	41.2	115.6	+21	+12%
	SHS89×3.5-F	F	-	122	1.06	12.8	49.9	-	-
SHS89×3.5 beams	CFT89×3.5-F-0	F	0	164	3.41	38.3	50.0	+42	+35%
	CFT89×3.5-F-15	F	15	155	4.74	26.2	99.3	+33	+27%
	CFT89×3.5-F-30	F	30	151	5.15	27.1	125.0	+29	+24%
	SHS100×3-F	F	-	109	0.65	10.2	40.1	-	-
SHS100×3 beams	CFT100×3-F-0	F	0	176	4.62	19.3	57.2	+67	+61%
	CFT100×3-F-15	F	15	162	7.70	17.9	94.6	+53	+48%
	CFT100×3-F-30	F	30	152	8.77	76.0	102.7	+43	+39%
	SHS100×2-F	F	-	59	0.53	8.8	30.1	-	-
SHS100×2 beams	CFT100×2-F-0	F	0	125	4.97	12.4	52.4	+66	+110%
	CFT100×2-F-15	F	15	111	8.16	17.0	61.6	+52	+87%
	CFT100×2-F-30	F	30	104	10.39	14.1	92.9	+45	+75%

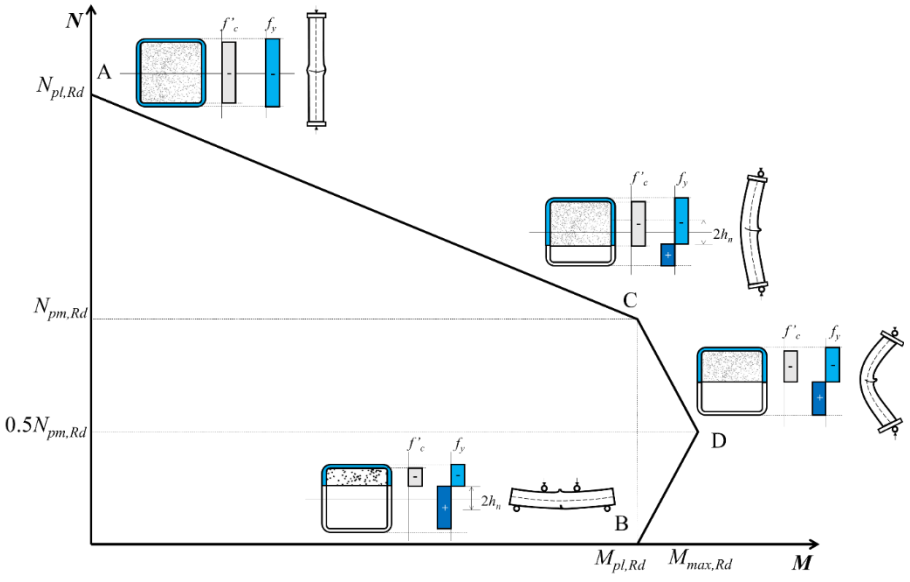

Fig. 2 The typical interaction diagram of the CFST members

At Point D, the load is half of that at Point C and the moment was the maximum (eq. 6).

$$M_D = M_{max,Rd} = W_{pa} f_y + 0.5 W_{pc} \alpha_c f_c' \quad (6)$$

The interaction diagrams of concrete filled SHS89×3.5 and SHS100×3 specimens constructed from the experimental results and theoretical calculations by Eurocode 4 [11] and CIDECT [12] are shown in Fig. 3 and 4, respectively. Overall, the behaviour of CFST specimens under combined loading conditions could be predicted at a reasonable accuracy and safe design could be produced. The position of the "balanced point" shifted downwards as the concrete compressive strength decreased. The interaction diagram tended to a straight line and shifted inwards as the steel contribution increased, as shown by the $A_s f_y/N_{pl,Rd}$ values in the figures.

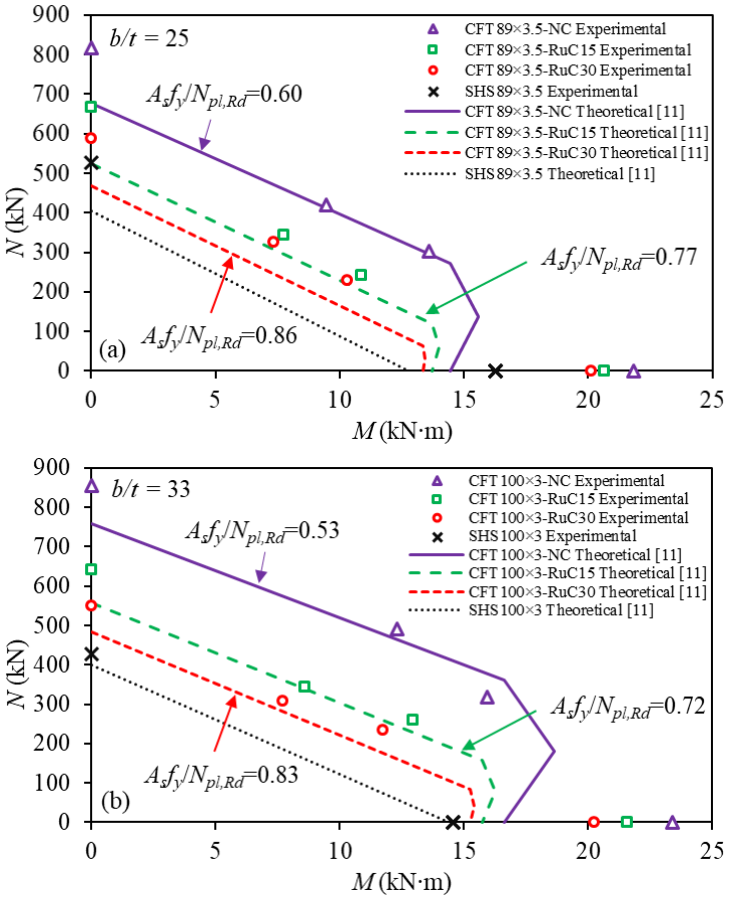

Fig. 3 The comparison between the experimental results and the analytical interaction diagram [11] of concrete filled (a) SHS89×3.5 and (b) SHS100×3 specimens

In Fig. 3a, the measured load carrying capacity of the concentrically loaded concrete filled SHS89×3.5 beams were safely underestimated by Eurocode 4 [11] by 24.4% on average. The compact steel section was more resistant to buckling and provided better confinement to the concrete core. The safety margin for the columns under combined loading conditions were considerably smaller than that for the concentrically loaded columns. The eccentrically loaded columns with NC were almost the same as theoretical predictions. RuC15 and RuC30 effectively delayed the buckling failure of the SHS tube, producing a satisfactory safety margin. The interaction diagrams showed the CFST beams were most favourable in bending, with the measured moment capacities well over the theoretical predictions by 50.7% on average. The projection of the hollow tubes was also given in the figure. As expected, the compact SHS89×3.5 had higher capacities than theoretical predictions, however still significantly lower than the CFST counterparts, especially in bending.

In Fig. 3b, the concentrically loaded columns confined by the non-compact SHS100×3 were still safe from a design point of view. The average safety margin was lower compared to those in the compact SHS89×3.5. For the eccentrically loaded columns, the interaction between the concrete and the outer tube still showed satisfactory confining and restraining effect by having a 13.7% increment over the theoretical predictions in Eurocode 4 [11]. The improvement was lower than that for the concrete filled SHS89×3.5 beams due to the higher section slenderness and the less effective confinement from the steel tube. The capacities of the eccentrically loaded CFST

columns were slightly overestimated, especially for NC at higher eccentricity. However, 30% RuCFST members could still be safely designed by Eurocode 4 [11]. Similar to concrete filled SHS89×3.5 beams, the beams with SHS100×3 failed in bending, resulting in higher (36.9%) bending capacity than the theoretical calculations. The safety margin of the hollow SHS100×3 beam was considerably smaller than the compact SHS89×3.5. This showed its higher tendency to buckle and less effective confinement to the concrete, which resulted in the lower safety margin of concrete filled SHS100×3 beams.

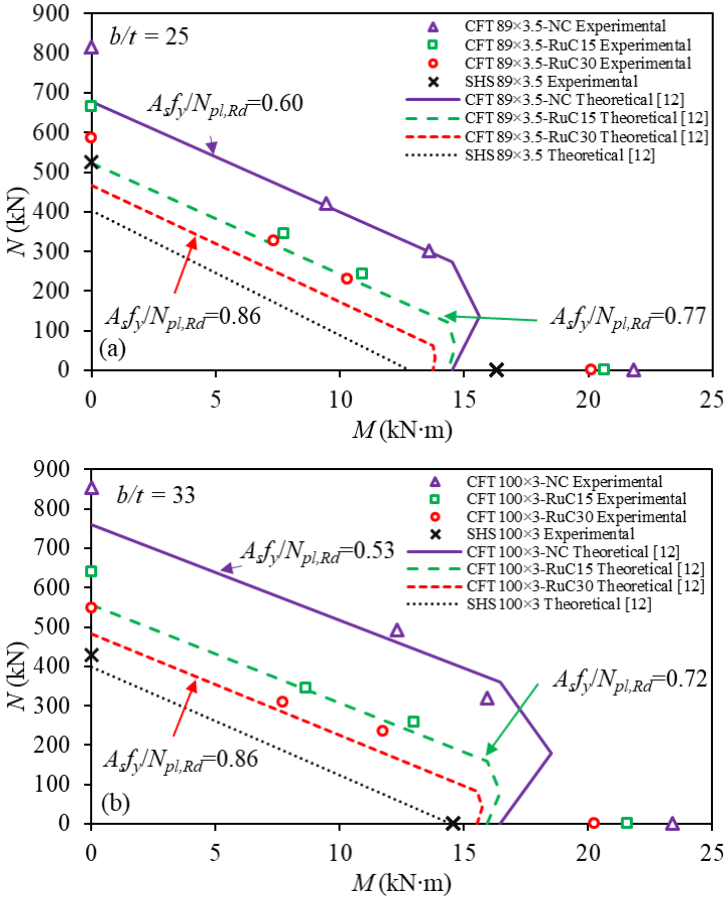

Fig. 4 The comparison between the experimental results and the analytical interaction diagram [12] of concrete filled (a) SHS89×3.5 and (b) SHS100×3 specimens

Fig. 4 showed the interaction diagram constructed as per CIDECT [12]. The overall interaction diagram was similar to Eurocode 4 [11], however it was slightly less conservative in terms of moment capacities and the contribution of concrete compressive strength in bending was lower. The CFST beams were still well above the calculated moment capacities, showing the effectiveness of using high ductility RuC as cost-effective infill.

Fig. 5 shows the normalised interaction diagram of the experimental results of the 24 concrete filled SHS89×3.5 and SHS100×3 specimens. The load N and moment M were normalised by the load and moment capacities of the hollow tubes. It could be seen from this figure that, the actual interaction diagram of the CFST specimens was approximately a linear relationship between the load and moment capacities. The more slender concrete filled SHS100×3 specimens were on the outer side due to the lower load and moment capacities of the hollow tube resulted from its higher tendency to buckle. The effect of compressive strength of the concrete infill was more profound for the slender SHS100×3. The weaker RuC15 and RuC30 were prone to crushing failure under large global deformation. However, RuC still offered significant improvement over the hollow section with low cost and improved sustainability. The effect of concrete compressive strength reduced as the load eccentricity increased, showing the potential of using RuCFST as cost-effective flexible roadside barriers.

4. Conclusions

Thirty CFST specimens with varying rubber content and steel section slenderness were tested under axial, flexural and combined loading conditions. The following conclusions could be drawn:

1) Higher rubber replacement ratios resulted in significant strength reduction of the concrete. However, the ductility of the concrete was greatly improved. As a concrete infill, RuC deformed to fill the buckles and effectively delayed the collapse.As a result, RuCFST members also showed improved ductility compared to their NCFST counterparts.

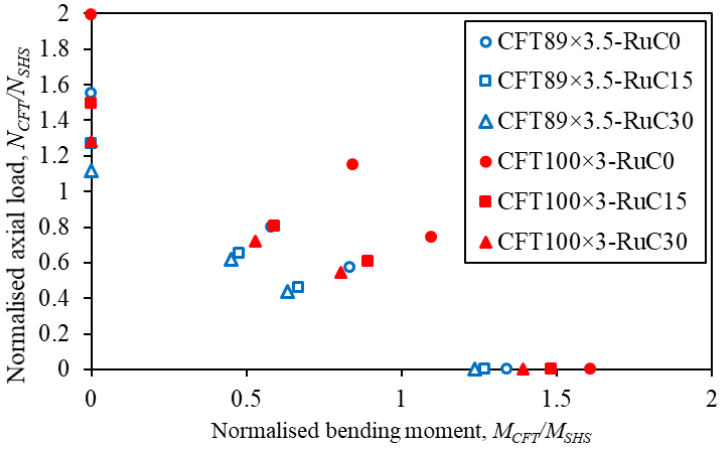

Fig. 5 The normalised interaction diagram of 24 CFST specimens

2) The strength deficiency of the RuC could be overcome by confinement through a steel tube. The improvement was even greater when the concrete was confined by a more compact section. The behaviours of the RuCFST members under combined loading could be accurately predicted using existing design guidelines for normal concrete.

3) CFST specimens with larger slenderness ratios showed larger ductility improvements compared with their hollow counterparts, due to their higher tendency to buckle.

4) It is recommended to confine RuC with steel tubular sections in the future construction as flexible roadside barriers and columns in buildings in seismic active zones.

5. Acknowledgements

The authors would like to deeply thank Liam O'keefe from Tyres Stewardship Australia and Adrian Jones from Tyrecycle. Thanks are given to Andrew Sarkady and Anup Chakrabortty from BASF for kindly donating the superplasticizer required for all the specimens. Thanks are given the following technicians Matt Arpin, Malcolm Stafford, Jim Waters and Brad Rose for assisting the students in performing the experiments. Thanks are given to Jaeyeol Park and Fiona Jones, students of UWA for performing the tests and processing the test data.

6. References

[1] Elchalakani M, Aly T, Abu-Aisheh E. Mechanical properties of rubberised concrete for road side barriers. Aust J Civ Eng. 2016;14:1–12. doi:10.1080/14488353.2015.1092631.
[2] Elchalakani M. High Strength rubberised concrete contains silica fumes for the construction of sustainable roadside barriers. Int J Struct. 2015;1:10–28.
[3] Duarte APC, Silva BA, Silvestre N, de Brito J, Júlio E, Castro JM. Tests and design of short steel tubes filled with rubberised concrete. Eng Struct. 2016;112:274–286. doi:10.1016/j.engstruct.2016.01.018.
[4] Elchalakani M, Hassanein MF, Karrech A, Yang B. Experimental investigation of rubberised concrete- filled double skin square tubular columns under axial compression. Eng Struct. 2018;171:730–746. doi:10.1016/j.engstruct.2018.05.123.
[5] Xue J, Shinozuka M. Rubberized concrete: A green structural material with enhanced energy-dissipation capability. Constr Build Mater. 2013;42:196–204. doi:10.1016/j.conbuildmat.2013.01.005.
[6] Zhao XL, Grzebieta R. Strength and ductility of concrete filled double skin (SHS inner and SHS outer) tubes. Thin-Walled Struct. 2002;40:199–213. doi:10.1016/S0263-8231(01)00060-X.
[7] Morino S, Uchikoshi M, Yamaguchi I. Concrete-filled steel tube column system-its advantages. Steel Struct. 2001;1:33–44.
[8] Segre N, Joekes I. Use of tire rubber particles as addition to cement paste. Cem Concr Res. 2000;30:1421–1425. doi:10.1016/S0008-8846(00)00373-2.
[9] AS 4100. Steel structures. 2nd ed. Standards Australia; 1998.

[10] EN 1993-1-1. Eurocode 3: Design of steel structures - Part 1-1: General rules and rules for buildings. 2005. doi:[Authority: The European Union Per Regulation 305/2011, Directive 98/34/EC, Directive 2004/18/EC].
[11] Eurocode 4. Eurocode 4: design of composite steel and concrete structures - Part 1.1: General rules and rules for buildings. 2004.
[12] CIDECT. Design guide for concrete filled hollow section columns under static and seismic loading. 1995.